Geochemical Perspectives Letters

Bacterial use of siderophores increases olivine dissolution rates by nearly an order of magnitude

A. Lunstrum[1*], M. Van Den Berghe[1], X. Bian[1], S. John[1], K. Nealson[1], A.J. West[1]

OPEN ACCESS

https://doi.org/10.7185/geochemlet.2315

Abstract

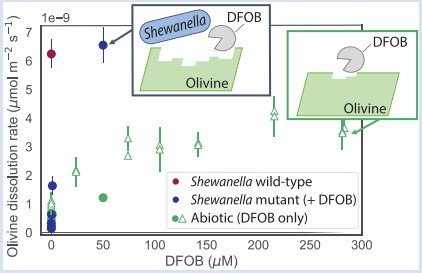

Mafic minerals, such as olivine, are an important source of metals and alkalinity to Earth's surface, impacting the planet's long term carbon cycle and climate. Yet, environmental controls on their dissolution rates remain poorly understood. Recent studies show that exogenous siderophores can enhance olivine dissolution abiotically, but it remains unclear how important siderophores are in microbially enhanced dissolution. Here, we isolated the effect of microbial siderophores on olivine dissolution using the bacteria *Shewanella oneidensis*, including both wild type and a mutant strain incapable of siderophore production. We show that *S. oneidensis* required siderophores to access mineral bound Fe, without which dissolution was not enhanced above background abiotic rates. Furthermore, dissolution rates with the bacteria were eight fold higher than those in abiotic solutions with the same concentrations of exogenous siderophores, implying a synergy between siderophores and other biotic mechanisms. After reaching stationary phase, dissolution in the *S. oneidensis* wild type treatment slowed, whereas that in the mutant + siderophore treatments continued at high rates. These results suggest that while siderophores are critical for biotically enhanced olivine dissolution, other microbe-related mechanisms magnify their effect.

Received 19 January 2023 | Accepted 4 April 2023 | Published 26 May 2023

Introduction

The chemical weathering of silicate minerals is an important control on global biogeochemical cycling and climate *via* the release of metal cations and alkalinity (White and Brantley, 1995). Improved understanding of the environmental controls on silicate dissolution is thus important for characterising the climate-weathering feedback (Berner *et al.*, 1983), and for informing engineered "enhanced weathering" efforts to mitigate climate change (Hartmann *et al.*, 2013). In this regard, olivine ($(Mg^{2+},Fe^{2+})_2SiO_4$) and olivine-rich rocks (such as basalt) are often studied as model silicates due to their high solubility, abundance, and resulting large contribution to earth's weathering flux (Dessert *et al.*, 2003; Hartmann *et al.*, 2009).

At Earth's surface, olivine dissolution kinetics can vary by orders of magnitude as a function of both abiotic and biotic environmental factors. The effect of abiotic conditions such as temperature, solution pH, and solution chemistry are relatively well constrained (Rimstidt *et al.*, 2012; Oelkers *et al.*, 2018). The effects of biology on dissolution rates, on the other hand, are less clear. While the net effect of biology on mineral dissolution is typically assumed to be positive, observed biotic effects range from inhibition to enhancement (Schwartzman and Volk, 1989).

Low molecular weight, multi-dentate ligands known as siderophores may be important drivers of microbially enhanced olivine dissolution. Siderophores are secreted by many bacteria, fungi, and grasses in response to Fe limitation. While they are structurally diverse, siderophores typically contain multiple metal-binding ligands that collectively result in exceptionally high binding affinity with Fe^{3+} ($\log K_f > 30$), preventing its loss from solution *via* Fe oxide precipitation (Hider and Kong, 2010). Significant research has shown that siderophores can *abiotically* enhance dissolution rates for a range of Fe^{3+} and Al^{3+}-containing minerals, including Fe oxides (Cheah *et al.*, 2003; Kraemer, 2004; Reichard *et al.*, 2007), Fe containing phyllosilicates (Rosenberg and Maurice, 2003; Haack *et al.*, 2008; Shirvani and Nourbakhsh, 2010; Ferret *et al.*, 2014; Bray *et al.*, 2015), and hornblende (Kalinowski *et al.*, 2000; Liermann *et al.*, 2000; Buss *et al.*, 2007). Olivine, in contrast, contains Fe almost exclusively in the +2 oxidation state, which is more weakly bound by siderophores (*e.g.*, for the siderophore deferoxamine B, $\log K_f = 30$ for Fe^{3+} *vs.* 10 for Fe^{2+}) (Dhungana and Crumbliss, 2005). Nonetheless, recent research has shown that siderophores also increase olivine dissolution rates by nearly an order of magnitude (Torres *et al.*, 2019). An important distinction, however, is that these studies use purified siderophores at high micromolar concentrations, whereas environmental concentrations are consistently much lower (pico- to nanomolar) (Kraemer, 2004). Thus, there remains a disconnect between our understanding of catalyst driven and biology driven mineral dissolution, and uncertainty as to whether siderophores are ultimately important drivers of dissolution in the environment (Brantley *et al.*, 2006).

This study attempts to clarify whether siderophores enhance olivine dissolution in biotic conditions (*i.e.* when actively utilised by microbes), and if so, if they are a requisite

1. Department of Earth Sciences, University of Southern California, Los Angeles, CA 90089, USA
* Corresponding author (email: lunstrum@usc.edu)

component of biotically enhanced dissolution. Specifically, we use sub-micromolar concentrations of siderophores — which do not significantly increase dissolution abiotically — to assess whether their active use by microbes increases mineral dissolution rates. While previous studies have found that siderophores are indeed critical for microbes to access or use mineral bound Fe, they have not linked this dependency quantitatively to mineral dissolution rates (Dehner *et al.*, 2010; Ferret *et al.*, 2014; Van Den Berghe *et al.*, 2021). Here, we focus specifically on this link between microbial use of siderophores and rates of mineral dissolution. To do so, we measured olivine dissolution rates in the presence of the bacteria *Shewanella oneidensis* (MR-1) wild type, and in the presence of a gene-deletion mutant of MR-1 incapable of producing siderophores (ΔMR-1) plus varying concentrations of the exogenous siderophore, deferoxamine B (DFOB). We furthermore compare these dissolution rates to abiotic rates with DFOB alone. While MR-1 is often studied for dissimilatory metal reduction, it was used in this study only due to availability of the siderophore gene-deletion mutant; dissimilatory Fe reduction was not a concern, as olivine bound Fe is almost exclusively in the +2 oxidation state (Van Den Berghe *et al.*, 2021).

Siderophores are Required for Biotically Enhanced Olivine Dissolution

In the absence of DFOB, ΔMR-1 could not access olivine bound Fe at rates fast enough to support growth, and correspondingly did not enhance mineral dissolution above well established abiotic rates (Figs. 1–3, S-1, Table S-1) (Rimstidt *et al.*, 2012). *S. oneidensis* has the capacity to take up Fe through alternative pathways not involving siderophores — including direct uptake of Fe^{2+} and/or ligand bound Fe^{3+} transport — so a dependence on siderophores for microbial growth is not obvious *a priori* (Liu *et al.*, 2018). Furthermore, alternative microbial processes, such as decreased pH or production of low molecular weight organic acids could also facilitate mineral dissolution to feed microbial growth (Wogelius and Walther, 1991). However, these processes may be insufficient to drive dissolution alone: ligand facilitated dissolution has been shown to be significant only at high ligand concentrations (typically >1 mM), which may not be achieved by slow growing microbes (Reichard *et al.*, 2007), and pH gradients in biofilms may not be severe enough to facilitate dissolution (Liermann *et al.*, 2000).

Similar studies using mutant *Pseudomonas* sp. grown in the presence of Fe^{3+} oxides and clays also found reduced growth rates in the absence of siderophores (Dehner *et al.*, 2010; Kuhn *et al.*, 2013; Ferret *et al.*, 2014). In contrast to our study, however, microbial growth was detectable without siderophores, indicating that alternative dissolution facilitating processes may be sufficient to facilitate some amount of microbial growth on Fe oxides and clays. The insignificant growth and dissolution in our ΔMR-1 (0 DFOB) treatment, on the other hand, indicates that siderophores are required to access olivine bound Fe. This difference suggests that Fe^{2+} bound within the olivine structure may be more difficult for microbes to access without siderophores than Fe^{3+} in oxides or clays.

Biotic Dissolution Rates exceed Abiotic Rates at the same Siderophore Concentration

It has been established that siderophores, independent of live culture, stimulate the dissolution of many Fe containing minerals, including olivine (Torres *et al.*, 2019). We show here, however, that live bacteria enhance this dissolution even further, beyond the rates expected for siderophore associated dissolution alone (Fig. 2, Table S-1). In all ΔMR-1 treatments where microbial growth was detectable (DFOB > 0.2 μM), dissolution rates exceeded those in abiotic conditions at the same DFOB concentration: at 1 μM DFOB addition, dissolution with ΔMR-1 exceeded the abiotic rate by three fold, and at 50 μM DFOB addition, this increased to eight fold. The enhanced dissolution observed in the biotic treatments implies that *S. oneidensis* does not simply benefit from passive use of siderophores, but rather, magnifies their efficiency.

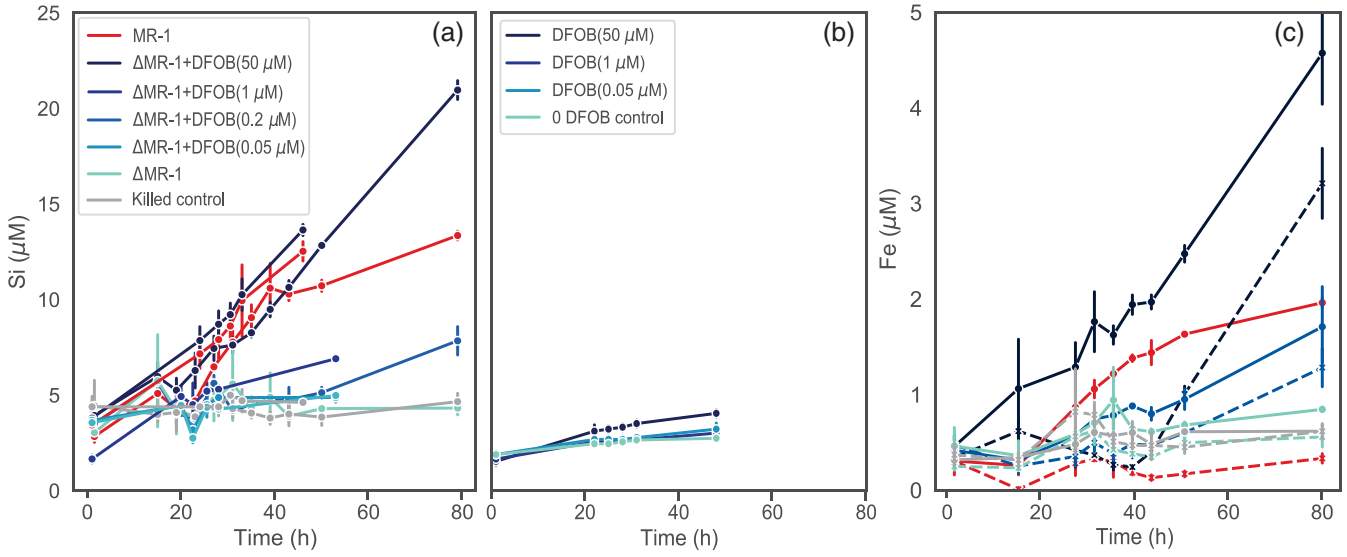

Figure 1 Dissolved Si measured in **(a)** biotic and **(b)** abiotic experiments, and **(c)** dissolved and total Fe in the biotic experiments (mean ± s.d.). Colours in all figures correspond to the same concentration of exogenous DFOB. Dashed lines in **(c)** represent dissolved concentrations, while solid lines are total concentrations.

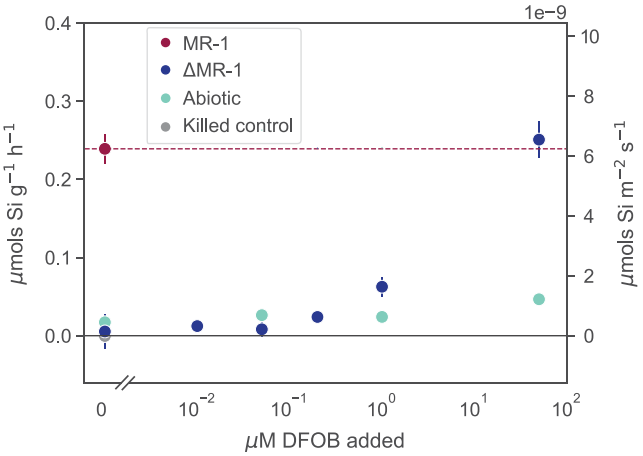

Figure 2 Olivine dissolution rates (based on Si release) as a function of DFOB addition. Dissolution rates in biotic treatments (ΔMR-1) exceed abiotic treatments at the same DFOB addition for DFOB > 1 μM. At 50 μM DFOB addition, biotic dissolution rates exceed abiotic rates by 8 fold. Dashed line represents dissolution rate for MR-1, with no exogenous siderophore addition.

Possible Mechanisms for Magnification of Siderophore Effects

One possible mechanism explaining higher rates in biotic *vs.* abiotic conditions is simply the microbial recycling of siderophores. In abiotic conditions, siderophores in solution can become saturated with chelated Fe. Active microbial populations, however, can transfer Fe to biomass, thus freeing siderophores for reuse. Our total *vs.* dissolved Fe data (Fig. 1c) support this mechanism, as Fe is almost entirely shunted into biomass, with no accumulation of chelated Fe in solution for the first 40 h of the ΔMR-1 experiments, and for the entirety of the MR-1 experiment. Even at 50 μM DFOB addition, which exceeds the concentration needed for maximum growth of ΔMR-1 (approximately 5 μM; Van Den Berghe *et al.*, 2021), chelated Fe does not accumulate in solution until well after stationary phase is reached, suggesting highly efficient siderophore use and shuttling of siderophore bound Fe into biomass.

However, mineral dissolution does not necessarily scale with siderophore *concentration*, but rather is known to scale with siderophores *adsorbed to the mineral surface*. As a result, dissolution rates plateau according to an adsorption isotherm. For DFOB, this has been well documented on olivine, Fe oxides and Fe containing phyllosilicates (Cheah *et al.*, 2003; Kraemer, 2004; Haack *et al.*, 2008; Torres *et al.*, 2019). Considering the relationship between olivine dissolution and DFOB concentration published by Torres *et al.* (2019) — which was derived at experimental conditions similar to ours (30 °C, pH 7.5) — dissolution rates plateau at >100 μM DFOB (Fig. 3). However, our measured dissolution rates for MR-1 and ΔMR-1 with only 50 μM DFOB addition are well above the bounds of the isotherm, suggesting that siderophore recycling alone does not fully explain biotic dissolution rates. Some other biotic mechanism likely facilitates increased siderophore efficiency. Siderophore adsorption to mineral surfaces is thought to be limited by both steric hindrance and charge repulsion (Cocozza *et al.*, 2002), so microbial secretion of surfactants or negatively charged ligands could increase adsorption efficiency (Carrasco *et al.*, 2007). Alternatively, small ligands like oxalate can interact synergistically with siderophores by liberating surface bound Fe when the saturation state of surrounding solution is lowered by siderophore mediated chelation of dissolved Fe (Cheah *et al.*, 2003; Reichard *et al.*, 2007). Of course, it is possible that a combination of these mechanisms collectively magnify siderophore efficiency.

Biotically Enhanced Dissolution persists with DFOB Addition, but Slows with Wild Type

When comparing the dissolution trends of MR-1 wild type and ΔMR-1 + DFOB (50 μM) treatments, three key observations stand out. First, dissolution rates are similar, despite ΔMR-1 achieving only 50 % of the wild type planktonic cell density (Figs. S-1, S-2). Second, dissolution in the wild type treatment slows after stationary phase is reached, whereas dissolution rates are constant in the ΔMR-1 treatments (Fig. 1a). And third, dissolved Fe begins to accumulate in the ΔMR-1 treatments during stationary phase, whereas dissolved Fe is completely absent in the wild type treatments (Fig. 1c). The fact that dissolution slows in the presence of MR-1 wild type can be explained by down regulation of siderophore production in response to Fe availability, a well established biofeedback mechanism in siderophore producers. In contrast, the unabated dissolution and accumulation of dissolved Fe in ΔMR-1 + DFOB experiments indicate that exogenous siderophores stimulate dissolution in excess of bacterial nutritional needs. Because dissolution continues at rates much higher than the abiotic DFOB rate, it can be inferred that the mechanism responsible for siderophore "magnification" is not limited by the same processes that down regulate siderophore production upon reaching stationary phase. Note that by the end of the experiment, dissolved Fe in the ΔMR-1 + DFOB (50 μM) treatment is only 3 μM. If not limited by other mechanisms, enhanced dissolution would likely continue until siderophores become saturated with Fe, *i.e.* up to 50 μM (Reichard *et al.*, 2007).

The fact that dissolved Fe does not accumulate in the MR-1 wild type treatment suggests that this bacterium uses siderophores extremely efficiently, shunting all *chelated* Fe into biomass. Considering the stoichiometry of total metal release,

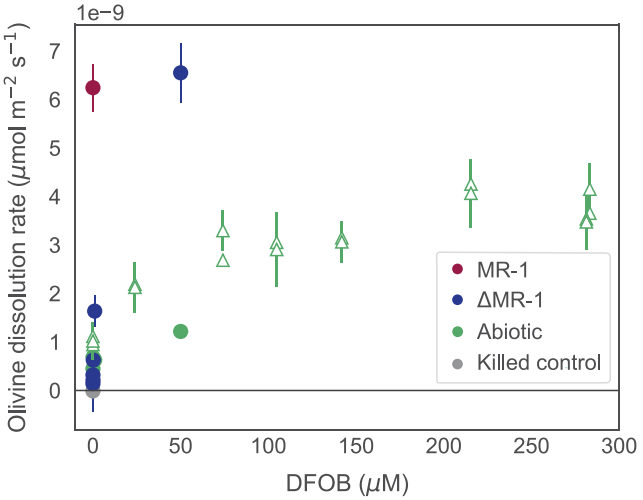

Figure 3 Olivine dissolution rates as a function of DFOB addition. Filled circles are from this study; hollow triangles are from Torres *et al.* (2019), adjusted to pH 7.2 as *per* the abiotic rate equations in Rimstidt *et al.* (2012). At 50 μM DFOB addition, our abiotic rate is reasonably characterised by (and slightly lower than) the abiotic adsorption isotherm. In contrast, the MR-1 and ΔMR-1 rates are significantly above the isotherm.

however, total Fe recovery in MR-1 was only 60 % of expected (based on Si release) at the end of the experiment, indicating that some dissolved Fe may escape chelation and be lost to secondary mineral precipitation (Fig. S-4). In contrast, the ΔMR-1 + DFOB treatments had full Fe recovery. The reduced Fe recovery and lack of dissolved Fe in MR-1 wild type experiments together suggest that siderophore production is low and/or localised at the microbe-mineral interface, with little siderophore loss to solution. Furthermore, a conundrum persists in that our previous research confirmed the presence of siderophores in MR-1 solution (using chrome-azurol S), and an experiment with ΔMR-1 fed filtrate from MR-1 exhibited normal growth patterns (Van Den Berghe *et al.*, 2021). It is possible that extremely low concentrations of *Shewanella*'s native siderophore putrebactin are sufficient to maintain the bacteria's growth and mineral dissolution needs, and that structural differences between putrebactin (a cyclic dihydroxamate) and DFOB (a tris-hydroxamate) allow for more efficient use in the former. The fact that MR-1 grows to stationary phase cell densities double those of ΔMR-1, yet dissolution rates are lower, further suggests that MR-1 uses available (chelated) Fe more efficiently with putrebactin.

Conclusions and Further Considerations

In conclusion, *Shewanella* does not use siderophores passively to enhance dissolution, but rather increases their efficiency to rapidly access mineral bound Fe. The observed biotically enhanced dissolution rates may not persist long term in natural conditions as they require the active biosynthesis of siderophores, which likely peak during exponential growth. Thus, significantly enhanced dissolution in the environment may be characteristic of non-stationary conditions, *e.g.*, when populations experience Fe limitation or other environmental perturbation (Reichard *et al.*, 2007). On the other hand, the continued high dissolution rates observed in the ΔMR-1 + DFOB treatments suggest that dissolution could persist in environments in which siderophores are present in excess of a given microbial group's growth needs, *e.g.*, when supplied by other bacteria, fungi, or plants. Similarly, the addition of exogenous siderophores, and/or microbes with altered genetic capabilities, may help maintain high dissolution rates in engineered conditions. These findings may be useful for engineering biotically mediated enhanced weathering systems, a nascent but potentially useful approach to increasing mineral dissolution rates. If dissolution rates can be maintained at 10× above abiotic rates, with minimal energy inputs, such geobiological approaches may be efficient methods for effective carbon dioxide sequestration.

Acknowledgements

This research was funded by the National Science Foundation, Division of Earth Sciences (EAR-1324929) and by the University of Southern California. We are also grateful to two anonymous reviewers for their helpful feedback.

Editor: Andreas Kappler

Additional Information

Supplementary Information accompanies this letter at https://www.geochemicalperspectivesletters.org/article2315.

Cite this letter as: Lunstrum, A., Van Den Berghe, M., Bian, X., John, S., Nealson, K., West, A.J. (2023) Bacterial use of siderophores increases olivine dissolution rates by nearly an order of magnitude. *Geochem. Persp. Let.* 25, 51–55. https://doi.org/10.7185/geochemlet.2315

References

Berner, R.A., Lasaga, A.C., Garrels, R.M. (1983) The Carbonate-Silicate Geochemical Cycle and Its Effect on Atmospheric Carbon Dioxide Over the Past 100 Million Years. *American Journal of Science* 283, 641–683. https://doi.org/10.2475/ajs.283.7.641

Brantley, S.L., Ruebush, S., Jang, J.-H., Tien, M. (2006) Analysis of (Bio) Geochemical Kinetics of Fe(III) Oxides. In: Maurice, P.A., Warren, L.A., Bain, D.C. (Eds.) *Methods for Study of Microbe-Mineral Interactions*. Clay Minerals Society Workshop Lectures v. 14, Clay Mineral Society, Chantilly, VA, 80–116. https://doi.org/10.1346/CMS-WLS-14.3

Bray, A.W., Oelkers, E.H., Bonneville, S., Wolff-Boenisch, D., Potts, N.J., Fones, G., Benning, L.G. (2015) The effect of pH, grain size, and organic ligands on biotite weathering rates. *Geochimica et Cosmochimica Acta* 164, 127–145. https://doi.org/10.1016/j.gca.2015.04.048

Buss, H.L., Lüttge, A., Brantley, S.L. (2007) Etch pit formation on iron silicate surfaces during siderophore-promoted dissolution. *Chemical Geology* 240, 326–342. https://doi.org/10.1016/j.chemgeo.2007.03.003

Carrasco, N., Kretzschmar, R., Pesch, M.-L., Kraemer, S.M. (2007) Low Concentrations of Surfactants Enhance Siderophore-Promoted Dissolution of Goethite. *Environmental Science & Technology* 41, 3633–3638. https://doi.org/10.1021/es062897r

Cheah, S.-F., Kraemer, S.M., Cervini-Silva, J., Sposito, G. (2003) Steady-state dissolution kinetics of goethite in the presence of desferrioxamine B and oxalate ligands: implications for the microbial acquisition of iron. *Chemical Geology* 198, 63–75. https://doi.org/10.1016/S0009-2541(02)00421-7

Cocozza, C., Tsao, C.C.G., Cheah, S.-F., Kraemer, S.M., Raymond, K.N., Miano, T.M., Sposito, G. (2002) Temperature dependence of goethite dissolution promoted by trihydroxamate siderophores. *Geochimica et Cosmochimica Acta* 66, 431–438. https://doi.org/10.1016/S0016-7037(01)00780-3

Dehner, C.A., Awaya, J.D., Maurice, P.A., DuBois, J.L. (2010) Roles of Siderophores, Oxalate, and Ascorbate in Mobilization of Iron from Hematite by the Aerobic Bacterium *Pseudomonas mendocina*. *Applied and Environmental Microbiology* 76, 2041–2048. https://doi.org/10.1128/AEM.02349-09

Dessert, C., Dupré, B., Gaillardet, J., François, L.M., Allegre, C.J. (2003) Basalt weathering laws and the impact of basalt weathering on the global carbon cycle. *Chemical Geology* 202, 257–273. https://doi.org/10.1016/j.chemgeo.2002.10.001

Dhungana, S., Crumbliss, A.L. (2005) Coordination Chemistry and Redox Processes in Siderophore-Mediated Iron Transport. *Geomicrobiology Journal* 22, 87–98. https://doi.org/10.1080/01490450590945870

Ferret, C., Sterckeman, T., Cornu, J.-Y., Gangloff, S., Schalk, I.J., Geoffroy, V.A. (2014) Siderophore-promoted dissolution of smectite by fluorescent *Pseudomonas*. *Environmental Microbiology Reports* 6, 459–467. https://doi.org/10.1111/1758-2229.12146

Haack, E.A., Johnston, C.T., Maurice, P.A. (2008) Mechanisms of siderophore sorption to smectite and siderophore-enhanced release of structural Fe^{3+}. *Geochimica et Cosmochimica Acta* 72, 3381–3397. https://doi.org/10.1016/j.gca.2008.03.027

Hartmann, J., Jansen, N., Dürr, H.H., Kempe, S., Köhler, P. (2009) Global CO_2-consumption by chemical weathering: What is the contribution of highly active weathering regions? *Global and Planetary Change* 69, 185–194. https://doi.org/10.1016/j.gloplacha.2009.07.007

Hartmann, J., West, A.J., Renforth, P., Köhler, P., De La Rocha, C.L., Wolf-Gladrow, D.A., Dürr, H.H., Scheffran, J. (2013) Enhanced chemical weathering as a geoengineering strategy to reduce atmospheric carbon dioxide, supply nutrients, and mitigate ocean acidification. *Reviews of Geophysics* 51, 113–149. https://doi.org/10.1002/rog.20004

Hider, R.C., Kong, X. (2010) Chemistry and biology of siderophores. *Natural Product Reports* 27, 637–657. https://doi.org/10.1039/b906679a

Kalinowski, B.E., Liermann, L.J., Givens, S., Brantley, S.L. (2000) Rates of bacteria-promoted solubilization of Fe from minerals: a review of problems and approaches. *Chemical Geology* 169, 357–370. https://doi.org/10.1016/S0009-2541(00)00214-X

Kraemer, S.M. (2004) Iron oxide dissolution and solubility in the presence of siderophores. *Aquatic Sciences* 66, 3–18. https://doi.org/10.1007/s00027-003-0690-5

Kuhn, K.M., DuBois, J.L., Maurice, P.A. (2013) Strategies of aerobic microbial Fe acquisition from Fe-bearing montmorillonite clay. *Geochimica et Cosmochimica Acta* 117, 191–202. https://doi.org/10.1016/j.gca.2013.04.028

Liermann, L.J., Kalinowski, B.E., Brantley, S.L., Ferry, J.G. (2000) Role of bacterial siderophores in dissolution of hornblende. *Geochimica et Cosmochimica Acta* 64, 587–602. https://doi.org/10.1016/S0016-7037(99)00288-4

Liu, L., Li, S., Wang, S., Dong, Z., Gao, H. (2018) Complex Iron Uptake by the Putrebactin-Mediated and Feo Systems in *Shewanella oneidensis*. *Applied and Environmental Microbiology* 84, e01752–18. https://doi.org/10.1128/AEM.01752-18

Oelkers, E.H., Declercq, J., Saldi, G.D., Gislason, S.R., Schott, J. (2018) Olivine dissolution rates: A critical review. *Chemical Geology* 500, 1–19. https://doi.org/10.1016/j.chemgeo.2018.10.008

Reichard, P.U., Kretzschmar, R., Kraemer, S.M. (2007) Dissolution mechanisms of goethite in the presence of siderophores and organic acids. *Geochimica et Cosmochimica Acta* 71, 5635–5650. https://doi.org/10.1016/j.gca.2006.12.022

Rimstidt, J.D., Brantley, S.L., Olsen, A.A. (2012) Systematic review of forsterite dissolution rate data. *Geochimica et Cosmochimica Acta* 99, 159–178. https://doi.org/10.1016/j.gca.2012.09.019

Rosenberg, D.R., Maurice, P.A. (2003) Siderophore adsorption to and dissolution of kaolinite at pH 3 to 7 and 22°C. *Geochimica et Cosmochimica Acta* 67, 223–229. https://doi.org/10.1016/S0016-7037(02)01082-7

Schwartzman, D.W., Volk, T. (1989) Biotic enhancement of weathering and the habitability of Earth. *Nature* 340, 457–460. https://doi.org/10.1038/340457a0

Shirvani, M., Nourbakhsh, F. (2010) Desferrioxamine-B adsorption to and iron dissolution from palygorskite and sepiolite. *Applied Clay Science* 48, 393–397. https://doi.org/10.1016/j.clay.2010.01.012

Torres, M.A., Dong, S., Nealson, K.H., West, A.J. (2019) The kinetics of siderophore-mediated olivine dissolution. *Geobiology* 17, 401–416. https://doi.org/10.1111/gbi.12332

Van Den Berghe, M., Merino, N., Nealson, K.H., West, A.J. (2021) Silicate minerals as a direct source of limiting nutrients: Siderophore synthesis and uptake promote ferric iron bioavailability from olivine and microbial growth. *Geobiology* 19, 618–630. https://doi.org/10.1111/gbi.12457

White, A.F., Brantley, S.L. (1995) *Chemical Weathering Rates of Silicate Minerals*. Reviews in Mineralogy v. 31, De Gruyter, Berlin, 583 p. https://doi.org/10.1515/9781501509650

Wogelius, R.A., Walther, J.V. (1991) Olivine dissolution at 25°C: Effects of pH, CO_2, and organic acids. *Geochimica et Cosmochimica Acta* 55, 943–954. https://doi.org/10.1016/0016-7037(91)90153-V

Geochemical Perspectives Letters

Bacterial use of siderophores increases olivine dissolution rates by nearly an order of magnitude

A. Lunstrum, M. Van Den Berghe, X. Bian, S. John, K.H. Nealson, A.J. West

Supplementary Information

The Supplementary Information includes:

- Methods
- Results
- Table S-1
- Figures S-1 to S-5
- Supplementary Information References

Methods

The experiment consisted of batch reactors containing olivine grains, Fe-deplete growth medium, and the following treatments: wild type *Shewanella oneidensis* (MR-1); a gene-deletion mutant of MR-1 incapable of producing siderophores (ΔMR-1); ΔMR-1 with added deferoxamine B (ΔMR-1 + DFOB, ranging from 0 to 50 µM); ΔMR-1 killed control; and abiotic treatments with no microbes but added DFOB (ranging from 0 to 50 µM). All treatments, listed in Table S-1, were conducted in triplicate. Henceforth, the live MR-1 and ΔMR-1 treatments are collectively referred to as "biotic", whereas the solutions with no microbial addition are referred to as "abiotic". Note that ΔMR-1 (*i.e.* ΔSO3031) was previously characterised as being incapable of producing siderophores but capable of utilising them through the hydroxamate reductase pathway (Fennessey *et al*., 2010). Furthermore, MR-1 is capable of taking up a range of siderophores, including the tris-hydroxamate DFOB, in addition to its native di-hydroxamate siderophore, putrebactin (Liu *et al*., 2018; Van Den Berghe *et al*., 2021).

Materials preparation. Olivine grains were collected from the University of Southern California mineral collection and were hand-crushed with a clean mortar and pestle. Crushed material was sieved to 150–300 µm diameter, ultrasonicated and rinsed seven times (5 min sonication *per* rinse) in 200-proof ethanol, then air-dried in an oven at 130 °C overnight. Immediately before the experiments, olivine grains were UV-sterilised for 30 min. Elemental composition of the olivine was analysed by X-ray fluorescence (XRF; Bruker S8 Tiger). By assuming a spherical shape and binning into six grain sizes with a normal distribution, the grain size distribution yielded a mean mineral surface area of 10,640 $mm^2\ g^{-1}$.

All experiments and sample analyses were performed in a laminar flow hood to prevent microbial and/or metal contamination. Furthermore, experiments and all media preparation were performed in acid-washed polycarbonate or polypropylene containers to avoid potential metal contamination from biotically induced glass dissolution (Gorbushina and Palinska, 1999; Aouad *et al*., 2006). The pH 7.2 growth medium was based on the M-1 minimal medium (Gorby *et al*., 2006), slightly modified by using MOPS buffer (50 mM) and N-acetyl glucosamine (18 mM) as the carbon source

and electron donor, in place of carboxylic acids that are known to enhance mineral dissolution abiotically (Neaman *et al*., 2005; Olsen and Rimstidt, 2008). Furthermore, Fe was omitted from the growth medium so that olivine was the only available Fe source. A detailed description of the growth medium composition is provided in Van Den Berghe *et al*. (2021). pH was confirmed at the beginning of the experiment and, given the high buffering capacity and relatively short duration of the experiment, was assumed to not change significantly over the course of the experiment.

For the biotic experiments, inoculation cultures were grown from individual isolated colonies and conditioned prior to the experiments in the same minimal medium (though Fe-replete, with 3.6 μM $FeSO_4$), without olivine. Microbes were extracted from these growth solutions by filtering (<0.2 μm), then triple-rinsed and concentrated in Fe-free medium prior to inoculation.

Batch reactor experiments. Batch reactor experiments were performed in Erlenmeyer flasks exposed to atmospheric conditions *via* porous caps, maintained in the dark at 30 °C, and shaken continuously at 120 rpm. 100 mL of the Fe-deplete medium was added to each flask, followed by inoculation cultures (for biotic experiments), and siderophore solution (for DFOB addition experiments). 100 mg olivine was then added to each flask. Flasks for the killed ΔMR-1 control treatment were autoclaved after inoculation, but prior to adding olivine.

For all biotic experiments, flasks were inoculated with approximately 5×10^{10} cells (for a starting cell concentration of approximately 5×10^{8} cells mL^{-1}). This initial cell density was selected to rapidly achieve maximum cell concentration. At each sampling time, 1 mL samples were extracted to monitor growth by optical density (OD) measurements, using pre-determined OD *vs*. cell count relationships (600 nm wavelength on Shimadzu UV-2600 spectrophotometer). Additional information on cell count methods is presented in Van Den Berghe *et al*. (2021).

For the ΔMR-1 + DFOB and abiotic DFOB treatments, a filter-sterilised stock solution of deferoxamine mesylate (Sigma Aldrich, US) was added to reach final concentrations ranging from 0.05 to 50 μM (Table S-1). A maximum of 50 μM was used based on prior findings that >5 μM DFOB addition was sufficient to stimulate maximum ΔMR-1 growth (Van Den Berghe *et al*., 2021). While DFOB is a tris-hydroxamate, structurally different from the cyclic di-hydroxamate putrebactin, it is known to be readily bioavailable to ΔMR-1.

Most experiments were run for approximately 48 h, just long enough for the biotic treatments to complete exponential growth and maintain stationary phase for ≥12 hours. A subset of experiments was run for 79 h to assess dissolution rates over a longer time period. Over the course of the experiments, samples were extracted (without volume replacement) for elemental analyses, ensuring homogenous sampling of suspended material by gently swirling bottles.

Elemental analysis of experimental solution. For experiments marked "OES" in Table S-1, dissolved Si was measured by inductively coupled plasma optical emission spectrometry (ICP-OES, Agilent 5100) at emission wavelengths of 251.611 nm. Because dissolved metal measurements in these experiments were either below ICP-OES detection (for Fe) or lower than the medium initial values (for Mg), we ran additional experiments for analysis of dissolved and solid phase metals by inductively coupled plasma mass spectrometry (ICP-MS, Thermofisher Scientific Element2); these are marked "ICP-MS, OES" in Table S-1.

For the OES only experiments, ~5 mL samples were taken at each timepoint, then filtered, acidified to ~0.5 % HNO_3, and preserved in the dark at 4 °C until analysis. Because Si does not have any biological function in *Shewanella* and is not a component of the minimal medium, dissolved Si was assumed to represent total dissolution flux from the mineral. For the ICP-MS, OES experiments, ~5 mL samples were taken at each timepoint, and separated into unfiltered and filtered (0.2 μm) aliquots. All samples were then acidified to 2 % HNO_3 and stored in the dark at room temperature until analysis. Prior to analysis, 100 μL aliquots were digested to prevent analytical interference by the organic matrix. Aliquots were added to PFA vials, acidified with 1 mL each of concentrated HCl and HNO_3, and dried at 120 °C overnight. Subsequently, dried samples were digested once more by adding 1 mL concentrated HNO_3, heating at 120 °C for 2–3 h, then drying at 120 °C overnight. Finally, samples were reconstituted with 1 mL 0.1 N HNO_3, with the addition of 10 ppb indium (In) as the internal standard to monitor analytical drift and correct for matrix effects. This multiple digestion procedure ensures the destruction of organic compounds and the complete dissolution of all available Fe. Measurements were taken for all metals present in the mineral (Table S-1). This digestion procedure resulted in significant Si loss, so additional aliquots of undigested, filtered samples were analysed for Si on the OES. For the OES analysis, 0.5 to 1 mL aliquots were reconstituted to 2.5 mL with Si-free growth medium, acidified to 2 % HNO_3, then analysed on the OES as described above.

Data analysis. All data analysis was performed in Python v 3.8.8.

Erroneous measurements were removed from the dataset *via* an automated quality control procedure based on replicate standard deviation, and/or obvious erroneous points (*e.g.*, unrealistically high or negative values) removed manually. Specifically, outliers were removed when triplicate standard deviation exceeded 50 % of the triplicate mean. This resulted, in for example, four Si data removed (out of 365), and 33 Fe data removed (out of 328). The higher rate of erroneous data with Fe is due to lower concentrations near analytical detection limits as well as higher probability of contamination during sample processing. Measured Si and metal concentrations at each timepoint (C_i) were corrected ($C_{i,\ \text{correct}}$) to consider mass extracted at prior timepoints: $C_{i,\text{correct}} = (C_i V_i + \sum_{j=1}^{(i-1)} v\, C_j)/V_0$ where V_i is the experimental volume remaining prior to sampling time i, v is the sample volume, C_j is the measured concentration at each prior timepoint, and V_0 is the initial experimental volume (100 mL).

Dissolution rates were inferred from changes in Si concentrations as Si, unlike Mg or Fe, is not used by *Shewanella* and is not a component of the minimal medium. Furthermore, Mg is highly exchangeable with protons at the initiation of dissolution experiments, and Fe easily precipitates as insoluble Fe-oxide secondary minerals, making both metals potentially misleading for calculation of net dissolution rate (Reichard *et al*., 2007; Oelkers *et al*., 2018). Dissolution rates were calculated based on the slope of corrected Si concentration *vs*. time ($\Delta Si/\Delta t$), considering only timepoints between 23 and 53 h, so as to exclude early timepoints with little microbial activity and later timepoints with significant accumulation of dead cells. This window captured the transition from exponential growth to stationary phase (Fig. S-2). These rates were normalised by either mineral mass (g^{-1}) or mineral surface area (m^{-2}). Rates were calculated for each bottle individually, then replicate bottles for the same treatment were averaged to yield a single dissolution value for each treatment. The dissolution rate for each treatment was considered statistically significant (*i.e.* significantly different from a rate of 0) if at least two of the three replicate bottles had p values <0.05.

Results

Olivine elemental composition. The cation composition of the ground olivine was 87.1 % Mg, 11.9 % Fe, and 0.5 % each of Ca and Ni, with trace amounts of Mn, Cr, Co, Zn, and Cu (Table S-1). The overall chemical composition is summarised as $Mg_{1.76}Fe_{0.24}SiO_4$ (*i.e.* Fo_{88}; predominantly forsterite with approximately 12 % Fe-containing fayalite in the solid solution).

Growth curves. Experiments with MR-1 and ΔMR-1 with added DFOB of at least 0.2 µM all exhibited exponential cell growth, reaching stationary phase between 24 to 40 h (Fig. S-1). Growth of the mutant ΔMR-1 scaled with DFOB addition, with no growth at DFOB < 0.2 µM, significant but inhibited growth with added DFOB between 0.2 and 1 µM, and maximum growth reached at 50 µM DFOB addition. Previous research using identical methods showed that cell density for ΔMR-1 maximises at approximately 5 µM DFOB addition, so ΔMR-1 + DFOB (50 µM) was not siderophore-limited (Van Den Berghe *et al*., 2021). Wild type MR-1 stationary cell density (8×10^9 cells mL^{-1}) was nearly double that of the ΔMR-1 + DFOB (50 µM) treatment (4×10^9 cells mL^{-1}).

Silicon and metal cation release rates. Dissolved Si was measurable in all samples, but the release rate during the stationary phase window considered was only significant for some treatments (Fig. 1a, b; Table S-1). In the abiotic treatments, Si release scaled with DFOB concentration, ranging from 0.02 to 0.04 µmol g^{-1} h^{-1}, and was significant for all DFOB additions, including the lowest concentration of 0.05 µM DFOB. In contrast, Si release in the ΔMR-1 + DFOB treatments was more variable and was not significant (at level of OES analytical detection) until at least 1 µM DFOB addition. Once detectable, Si release rates in the biotic treatments were higher than in the abiotic treatments at the same DFOB concentration, reaching 0.27 µmol g^{-1} h^{-1} in the ΔMR-1 + DFOB (50 µM) treatment. Si release in wild type MR-1 was comparably high, reaching 0.25 µmol g^{-1} h^{-1}. The change in Si release rate over time also varied between biotic and abiotic experiments. In abiotic conditions, Si release was fastest between 0 and 24 hours, followed by relatively slower rates, similar to other abiotic experiments with siderophores (Torres *et al*., 2019). In contrast, the biotic experiments typically had relatively constant release rates during the measurement period, and if anything, slower initial rates. However, wild type MR-1 uniquely exhibited a slowing of Si release rates shortly after reaching stationary phase, after approximately 40 h.

Total Fe release closely mirrored Si, with increasing Fe in all biotic treatments with siderophore addition (Fig. 1c). For the time period considered (23–53 h), however, release rates were only significant in the MR-1 and ΔMR-1 + DFOB (50 μM) treatments. Considering the later timepoint, ΔMR-1 + DFOB (0.2 μM) also had a significant Fe release rate. The ΔMR-1 + DFOB (50 μM) treatment showed a consistent release rate of 0.05 μmol g^{-1} h^{-1}, whereas the release rate for MR-1 wild type was initially similar, but slowed after stationary phase was achieved at 40 h. Prior to 40 h, there was no significant dissolved Fe in any treatment, implying the total Fe increase was entirely shunted to biomass. (In this study, we assume particulate Fe and Mg to be in biomass. While it is possible that metals may adsorb to cell exteriors, a distinction between internal or adsorbed Fe does not affect our analysis.) In the MR-1 treatment, dissolved Fe remained near zero for the duration for the experiment. However, in all ΔMR-1 treatments, dissolved Fe increased after 40 h, following the total Fe trend, implying accumulation of Fe in dissolved phase but no change in the particulate Fe pool.

In contrast to Si, total Mg was initially stable or decreased slightly, followed by an increase after approximately 24 h (Fig. S-3). Only the ΔMR-1 + DFOB (50 μM) treatment showed sustained Mg release through the end of the experiment, whereas Mg concentrations in the other treatments stabilised after about 40 h. Replicate variability for these latter timepoints was relatively high, however, precluding clear trends. Considering dissolved Mg, both biotic treatments with high growth rates (MR-1 and MR-1Δ + DFOB (50 μM)) showed a significant reduction in dissolved Mg during the exponential growth phase, with an increase in dissolved Mg thereafter.

Compared to the known mineral stoichiometry, elemental ratios of Si, Mg, and Fe showed disproportionate Si release for the first ~30 h of the experiment (Fig. S-4a, b). After 40 h, Mg release increased for all treatments and Mg/Si appeared to remain congruent for the duration of the experiment, although sample error was high. Total Fe followed a similar pattern for the ΔMR-1 treatments, with congruent Fe/Si after approximately 30 h. For the MR-1 and control treatments, however, Fe/Si remained depressed at about 60 % of expected stoichiometry.

For trace metals, only Ni exhibited any significant release, and then only for the ΔMR-1 + DFOB (50 μM) treatment, with a release rate of 0.004 ± 0.001 μmol Ni g olivine^{-1} h^{-1} (Fig. S-5). Dissolved and total Ni concentrations were similar, implying that Ni was not taken up by, or adsorbed to, biomass. All other metals showed no trends over time that exceeded analytical uncertainty.

Supplementary Table

Table S-1 Experimental details and elemental release rates for Si and Fe (mean ± s.d.). '--', not measured; *n.s.*, not significantly different from 0.

Category	Treatment	DFOB (µM)	Experiment Length (h)	Analysis	Si release (µmol g^{-1} h^{-1})	Fe release (µmol g^{-1} h^{-1})
Biotic	MR-1	0	79	ICP-MS, OES	0.23 ± 0.01	0.04 ± 0.01
	MR-1	0	46	OES	0.25 ± 0.02	--
	ΔMR-1	0	79	ICP-MS, OES	*n.s.*	*n.s.*
	ΔMR-1	0	53	OES	*n.s.*	--
	ΔMR-1 + DFOB	0.05	53	OES	*n.s.*	--
	ΔMR-1 + DFOB	0.2	79	ICP-MS, OES	*n.s.*	*n.s.*
	ΔMR-1 + DFOB	1	53	OES	0.06 ± 0.01	--
	ΔMR-1 + DFOB	50	79	ICP-MS, OES	0.23 ± 0.01	0.05 ± 0.01
	ΔMR-1 + DFOB	50	46	OES	0.27 ± 0.01	--
Abiotic	Killed ΔMR-1	0	79	ICP-MS, OES	*n.s.*	*n.s.*
	Killed ΔMR-1	0	46	OES	*n.s.*	--
	Control	0	48	OES	*n.s.*	--
	DFOB	0.05	48	OES	0.02 ± 0.01	--
	DFOB	1	48	OES	0.02 ± 0.01	--
	DFOB	50	48	OES	0.04 ± 0.01	--

Supplementary Figures

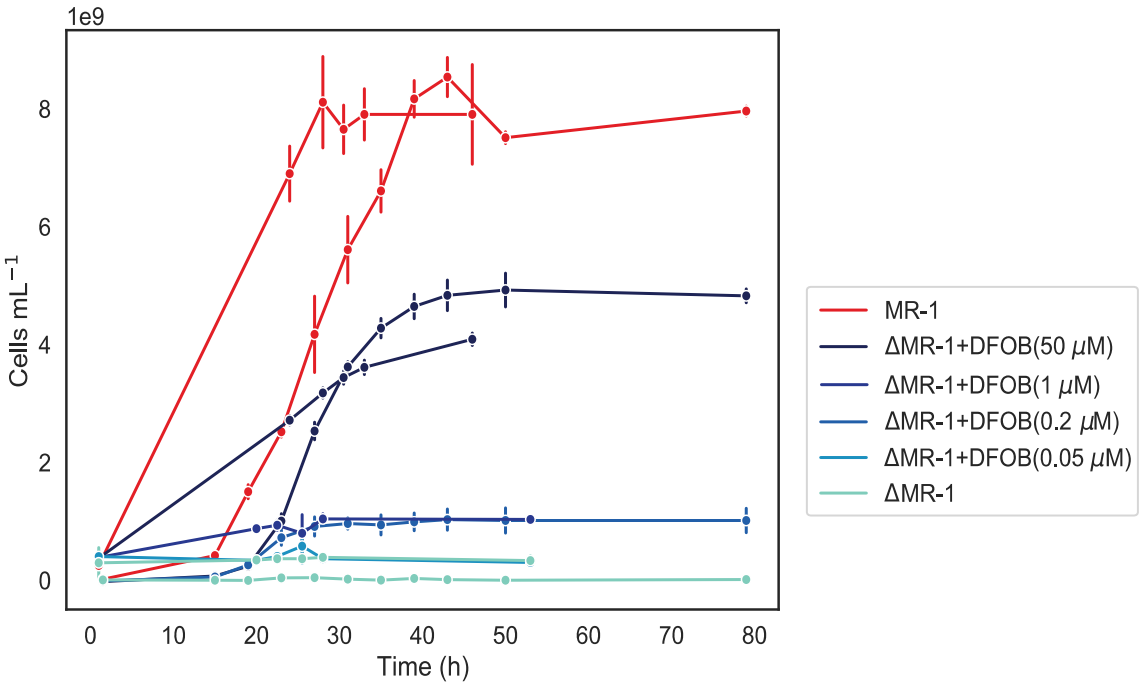

Figure S-1 Growth curves for all biotic treatments. For ΔMR-1 treatments, darker blue shades indicate increasing DFOB addition. All experiments performed in triplicate (error bars are standard deviation). The MR-1 and ΔMR-1 + DFOB (50 μM) experiments were conducted twice; each experimental batch is shown as a separate line in the figure.

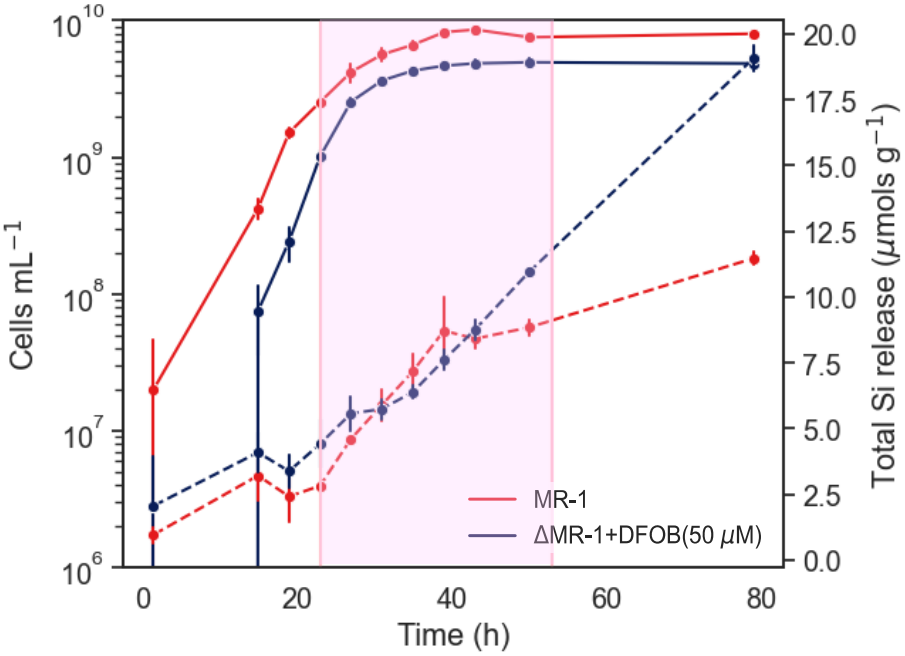

Figure S-2 Examples of growth curves (solid lines, with log-*y* axis) and total Si release (dashed lines) for MR-1 and ΔMR-1 + DFOB (50 µM) experiments. The time-period used to calculate dissolution rates (23 to 53 h) isolates the onset of stationary phase, as highlighted in pink.

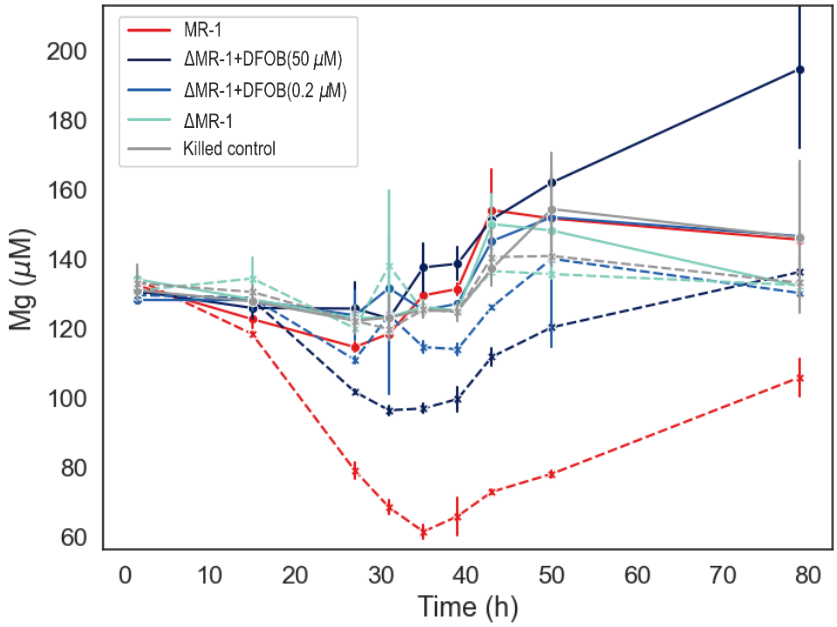

Figure S-3 Dissolved and total Mg *versus* time for the subset of experiments analysed by ICP-MS (mean ± s.d.). Solid lines represent total (unfiltered) elemental release, and dashed lines represent the dissolved (filtered) component.

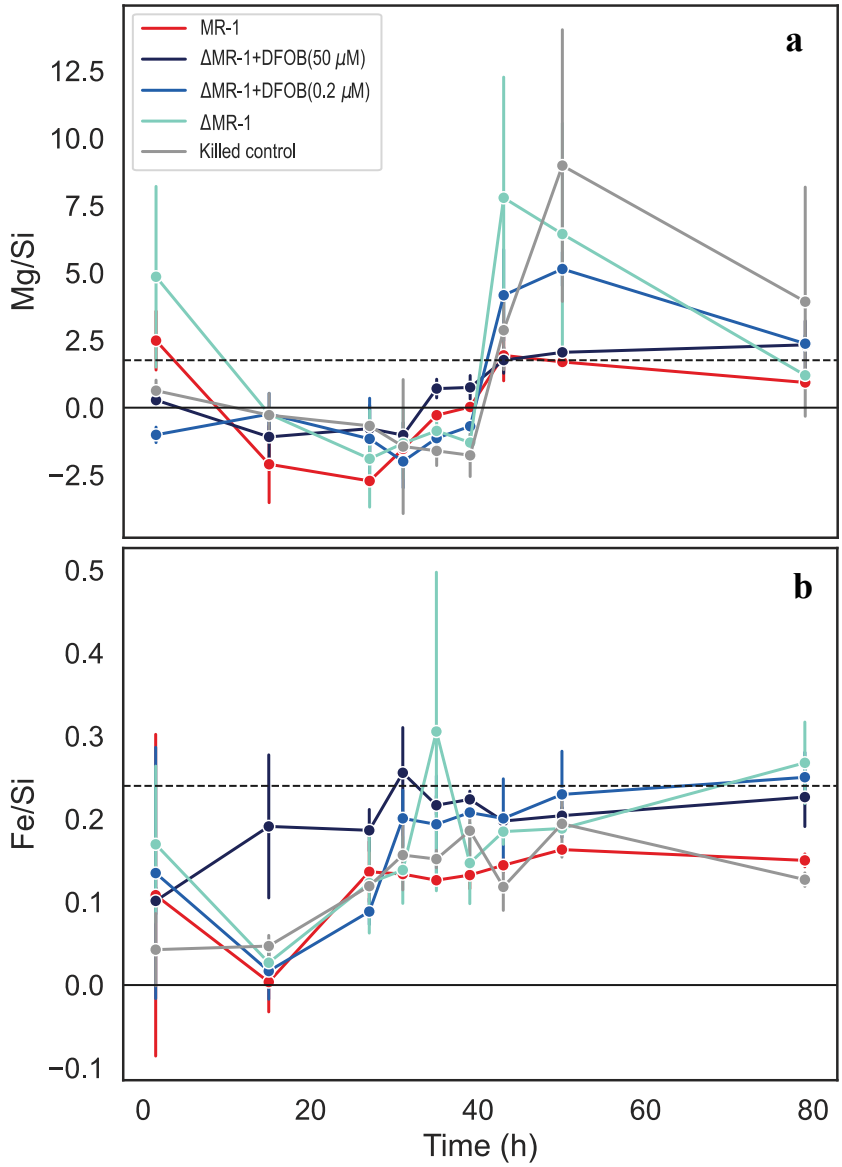

Figure S-4 Elemental ratios of **(a)** total Mg to dissolved Si release and **(b)** total Fe to dissolved Si release *versus* time. Dissolved Si is assumed equivalent to total Si. Dashed lines represent stoichiometry of the source olivine. All experiments performed in triplicate (error bars are standard deviation).

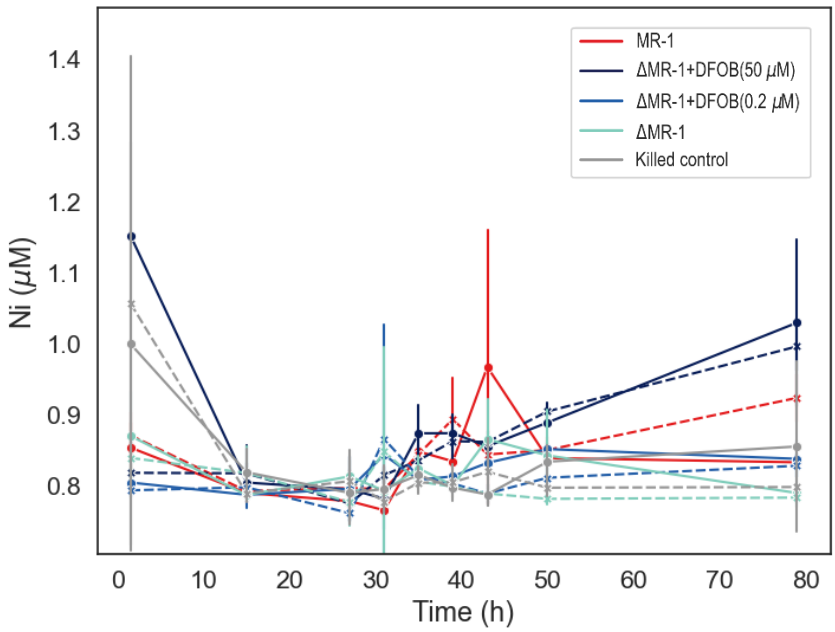

Figure S-5 Dissolved and total Ni *versus* time for the subset of experiments analysed by ICP-MS (mean ± s.d.). Solid lines represent total (unfiltered) elemental release, and dashed lines represent the dissolved (filtered) component. Only the ΔMR-1 + DFOB (50 μM) had a statistically significant Ni release rate.

Supplementary Information References

Aouad, G., Crovisier, J.-L., Geoffroy, V.A., Meyer, J.-M., Stille, P. (2006) Microbially-mediated glass dissolution and sorption of metals by *Pseudomonas aeruginosa* cells and biofilm. *Journal of Hazardous Materials* 136, 889–895. https://doi.org/10.1016/j.jhazmat.2006.01.026

Fennessey, C.M., Jones, M.E., Taillefert, M., DiChristina, T.J. (2010) Siderophores Are Not Involved in Fe(III) Solubilization during Anaerobic Fe(III) Respiration by *Shewanella oneidensis* MR-1. *Applied and Environmental Microbiology* 76, 2425–2432. https://doi.org/10.1128/AEM.03066-09

Gorbushina, A.A., Palinska, K.A. (1999) Biodeteriorative processes on glass: experimental proof of the role of fungi and cyanobacteria. *Aerobiologia* 15, 183–192. https://doi.org/10.1023/A:1007616614172

Gorby, Y.A., Yanina, S., McLean, J.S., Rosso, K.M., Moyles, D., *et al*. (2006) Electrically conductive bacterial nanowires produced by *Shewanella oneidensis* strain MR-1 and other microorganisms. *Proceedings of the National Academy of Sciences* 103, 11358–11363. https://doi.org/10.1073/pnas.0604517103

Liu, L., Li, S., Wang, S., Dong, Z., Gao, H. (2018) Complex Iron Uptake by the Putrebactin-Mediated and Feo Systems in *Shewanella oneidensis*. *Applied and Environmental Microbiology* 84, e01752-18. https://doi.org/10.1128/AEM.01752-18

Neaman, A., Chorover, J., Brantley, S.L. (2005) Implications of the Evolution of Organic Acid Moieties for Basalt Weathering Over Geological Time. *American Journal of Science* 305, 147–185. https://doi.org/10.2475/ajs.305.2.147

Oelkers, E.H., Declercq, J., Saldi, G.D., Gislason, S.R., Schott, J. (2018) Olivine dissolution rates: A critical review. *Chemical Geology* 500, 1–19. https://doi.org/10.1016/j.chemgeo.2018.10.008

Olsen, A.A., Rimstidt, J.D. (2008) Oxalate-promoted forsterite dissolution at low pH. *Geochimica et Cosmochimica Acta* 72, 1758–1766. https://doi.org/10.1016/j.gca.2007.12.026

Reichard, P.U., Kretzschmar, R., Kraemer, S.M. (2007) Dissolution mechanisms of goethite in the presence of siderophores and organic acids. *Geochimica et Cosmochimica Acta* 71, 5635–5650. https://doi.org/10.1016/j.gca.2006.12.022

Torres, M.A., Dong, S., Nealson, K.H., West, A.J. (2019) The kinetics of siderophore-mediated olivine dissolution. *Geobiology* 17, 401–416. https://doi.org/10.1111/gbi.12332

Van Den Berghe, M., Merino, N., Nealson, K.H., West, A.J. (2021) Silicate minerals as a direct source of limiting nutrients: Siderophore synthesis and uptake promote ferric iron bioavailability from olivine and microbial growth. *Geobiology* 19, 618–630. https://doi.org/10.1111/gbi.12457